An Investigation Into The Energy Efficiency of Digital Micrography Based Toolpaths

by

Jeronimo Mora

A report submitted in partial satisfaction of the
requirements for the degree of
Master of Science, Plan II

in

Mechanical Engineering

in the

Graduate Division

of the

University of California, Berkeley

Committee in charge:

Professor Sara McMains, Chair
Professor Hayden Taylor

Summer 2018

An Investigation Into The Energy Efficiency of Digital Micrography Based Toolpaths

Abstract

An Investigation Into The Energy Efficiency of Digital Micrography Based Toolpaths

by

Jeronimo Mora

Master of Science, Plan II in Mechanical Engineering

University of California, Berkeley

Professor Sara McMains, Chair

Initial research on vector field based toolpaths for CNC pocket machining recently showed them to be more energy efficient than commercially available toolpath approaches. This report presents improvements to the vector field based toolpath approach and present machining experiments in order to further investigate the efficiency of the approach. The report presents toolpath comparisons for different geometries and presents machining experiments to compare the energy consumption of toolpaths aligned with different primary axes. The current iteration of the vector field based toolpath approach discussed in this report is inferior to commercial toolpath approaches. This report proposes several improvements to this toolpath approach that may make it more viable.

Energy efficient CNC toolpaths; CNC machining; Toolpath planning.

Acknowledgments

This material is based upon work supported by the National Science Foundation Graduate Research Fellowship Program under Grant No. DGE-1752814. I would like to thank the UC Berkeley Machine Shop staff for help with CAM software and for providing some stock material. In particular, I want to extend special thanks to Jesus Lopez for his patience, expertise, and help running the milling experiments. I would like to acknowledge Nathan Carr of Adobe, Professor Alla Sheffer of the University of British Columbia, and Ron Maharik for working on and providing the code for performing digital micrography, and for granting permission to reuse a figure they created in this work (reprinted by permission of ACM). I would like to thank my advisor Professor Sara McMains for her support and guidance throughout my time in graduate school. Lastly, I'd like to thank my wife for tolerating my commute and supporting me throughout this endeavor. Go Bears!

Contents

List of Figures

List of Tables

Chapter 1

Introduction

The industrial sector is one of the largest consumers of energy in the United States, consuming approximately 32% of the total energy consumed in 2016 (*U.S. Energy Facts - Energy Explained* 2017). Metal products and metal processing account for approximately 10 % of the industrial sector's energy use. (*U.S. Energy Facts - Energy Explained* 2018). Given that such a colossal portion of the United States' total energy consumption goes to manufacturing, it is easy to see why companies and researchers are interested in increasing the energy efficiency of manufacturing processes. CNC machining is one of the more traditional and widely used manufacturing processes. Electricity in a CNC machine is used to power the motors, fans, electronics, and cooling equipment. These electrical costs can be roughly divided into two groups:

1. Electrical costs that scale with machining time
2. Electrical costs that depend on material removal

As the complexity of a machine grows, the electrical costs that scale with time can increase relative to costs associated with material removal (Kordonowy, 2002; Pavanaskar, 2014). This leads to a strong correlation of energy use and processing time. The choice of an appropriate toolpath will be a deciding factor in the process cycle time, and will therefore play a large role in determining the process energy efficiency. Some researchers reported a novel approach to generating inherently energy efficient CNC pocket machining toolpaths based on vector field streamlines (Pavanaskar et al., 2015). The initial results were promising and demonstrated energy savings of 20 - 30% when compared to commercial toolpaths. This report takes a closer look at this approach to toolpaths, presents improvements to the toolpath generation and presents machining experiments on a 3-axis vertical milling machine to analyze its energy efficiency.

1.1 Background

Energy Consumption in CNC Machines

Before delving into approaches that have been used to reduce the energy consumption in CNC machines, it is important to understand the energy characteristics of the CNC machining process. Researchers Y. He et al. performed an analysis of the energy consumption of a CNC machine (2012). They first estimated the energy consumption of the machine using an energy model and then performed a case study to validate their estimations. Their energy model in its base form is straight-forward to understand. The total energy consumed in a machining process is simply the sum of all the energy consumed in sub-systems and sub-processes. Their model can be represented as

$$E_{total} = E_{spindle} + E_{feed} + E_{tool} + E_{cool} + E_{fix} \tag{1.1}$$

where the total energy consumed is comprised of the spindle energy, feed energy, tool change energy, cooling system energy, and the non-variable energy consumed in a process. Each of these items can be further subdivided into greater detail; however, they will not be discussed here. When modeled for a vertical-milling machine, the researchers were able to estimate the percentages of energy usage. According to their estimates nearly 75 % of the energy use is expended by fans and the coolant system. A study of "environmentally benign manufacturing" presented data provided by Toyota Motor Corporation that showed that their machining operations had a "constant" (non-machining) energy cost that was 85.2 % of the total energy usage (Gutowski et al., 2005). The energy cost required to run the machines themselves is a significant portion of the total process energy. Researchers have shown that the energy consumption for large volume machines is dominated by machining time (Diaz, Redelsheimer, and Dornfeld, 2011). It can be seen in Appendix Figures 5.1 and 5.2 that the CNC machine used in this report consumes approximately 1000W solely by virtue of being on. The standby energy consumption is almost as high as the energy consumption of the machine during air-cutting with fluid (1500W).

Energy Efficient Toolpath Approaches

When looking for ways to reduce the energy consumption of CNC machining, the choice of toolpath is an obvious place to begin. With energy correlated so closely with time, toolpaths that finish the machining process faster are often (but not always) more energy efficient. Work has shown that when CNC machining, the direction of travel can greatly affect the energy consumption of a machining operation. If a machine is configured such that the X axis is mounted on top of the Y axis, then moving the Y axis will also require moving the entire X axis. In most cases this will result in the Y axis requiring more energy to move than the X axis for an equivalent distance. Toolpaths whose machining direction is aligned with the direction of "minimal moving weights" will be more energy efficient (Tonissen, 2009). Some researchers have compared a true spiral toolpath with a high speed dynamic (HSD) toolpath

and found that while the HSD toolpath had a higher mean power consumption, the cycle time was significantly lower, saving close to 62% of the energy spent machining using a true spiral (Minquiz et al., 2016). Reducing the amount of idle time and air-cutting will reduce the energy consumption of the machine. Researchers have proposed using the Medial Axis Transformation of a pocket to calculate efficient spiral toolpaths that were shown to save anywhere from 1 to 40% of machining time compared to standard spiral toolpaths generated from a CAM package. The amount of energy saved depended on the geometry of the pocket (Huang, Lynn, and Kurfess, 2017). The vector field based toolpaths designed by Pavanaskar et al. drew influence from digital art (2015). The researchers used streamlines generated by software written by Maharik et al. meant for digital micrography (2011) (art where text or words form an image when viewed from away) to generate toolpaths for CNC pocket machining. They compare the micrography based toolpath to other toolpaths generated by a CAM software package (zigzag, X-parallel, spiral etc.) and demonstrate energy savings of 20.6% to 35.3%. The process of digital micrography is discussed in the next subsection.

Digital Micrography

Digital micrography is a digital art form where bodies of text are placed in such a fashion so as to create a shape out of the words. The text positioning is determined by generating streamlines traced from a smooth vector field. In order for the text layout to be legible, aesthetically pleasing, and true to the boundary shape, the vector field is generated in such a fashion that it is selectively aligned with the boundary. This allows the streamlines to have long segments and exhibit low curvature. The different regions and streamlines are also put into an order so that when the text is placed, the order will be logical for a reader.

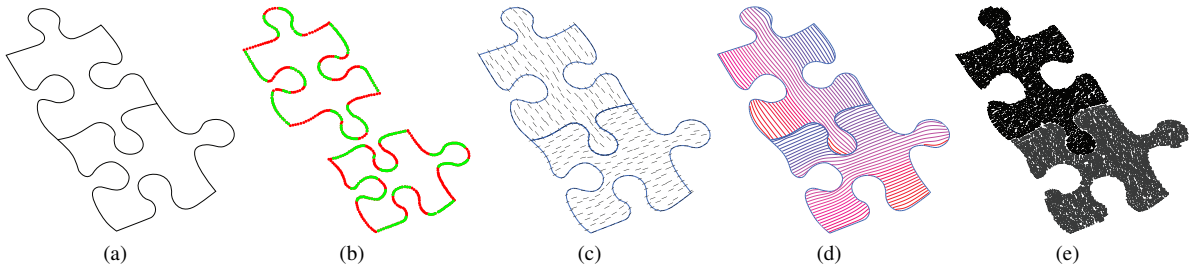

Figure 1.1: The micrography process. (a) Boundary information is collected and (b) boundary weights are calculated. (c) A vector field is generated from which (d) streamlines are traced for (e) text layout. (Maharik et al., 2011) © 2011 Association for Computing Machinery, Inc. Reprinted by permission.

Digital Micrography Process

An example of the micrography process is provided in Figure 1.1 above. The digital micrography process begins with either sampling the region boundary paths, or reading in the region boundary information. Each region is then triangulated and the triangulation is converted to a mesh. The boundary vertices are given weights that are initialized and then optimized. The boundary weights are optimized such that the vector field will align with the boundary; however, these restrictions are selectively relaxed to avoid regions of high curvature and promote longer lengths for the streamline segments. Once the boundary weights are optimized, a 2-RoSy (two way rotational symmetry) vector field (Palacios and Zhang, 2007) is generated in the region. Streamlines are generated by tracing the vector field. The streamlines undergo some post-processing that can include deleting very short streamlines and combining nearby aligned streamlines. The streamlines may not be equally spaced, so they undergo a process of optimization where the streamline spacing is equalized as much as possible. With the streamlines processed, they are given an orientation that is determined by graph search techniques. This orientation along with position information is used to topologically sort (order) the streamlines for text layout. Finally, once an ordering has been found, the text is placed in the region and warped to fill the gaps in the case that the distance between streamlines is non-uniform.

Chapter 2

Methods

2.1 Generating Micrography Based Toolpaths

The following subsections describe methods of generating streamlines for digital micrography and turning those into CNC toolpaths. The software that generates the streamlines used for the CNC toolpaths was written by Maharik et al. at the University of British Columbia and Adobe Systems Inc. The original method of turning streamlines into toolpaths as reported by Pavanaskar et al. will from here on out be referred to as the version 0 (V0) micrography approach. I have made several improvements that are described below. The improved aproach is referred to from here on out as the version 1 (V1) micrography approach.

Generating Streamlines

Given the boundary information for a pocket, the first step to generating a toolpath based on digital micrography is to generate the streamlines. The V0 and V1 toolpath software first calls the micrography software with the boundary information, a Boolean representing whether line ordering is desired, and a spacing variable, which for micrography will represent the font size, as input. The approximate streamline spacing distance is given as a function of font size. This is because for micrography the streamlines need to be far enough apart to allow the body of text to not overlap. The parameter that scales the input font size can be changed to allow for custom stepover distances. The stepover distance is the distance between successive toolpath passes (see Figure 2.1). Giving the micrography software the tool diameter as the font size and the scaling parameter as 0.5 results in streamlines that are roughly a tool radius away from each other. Once the code is done generating streamlines, it samples and stores each streamline as a set of closely spaced vertices that approximate the streamline in a piecewise-linear fashion. For the remainder of the report, I will refer to S as the set of all streamlines $\{s_0, s_1, s_2, ..., s_n\}$ and to each individual streamline s_i as the set of all its vertices $\{v_0, v_1, v_2, ..., v_n\}$. If using line ordering is desired, the micrography code will also perform the topological sorting and save the result.

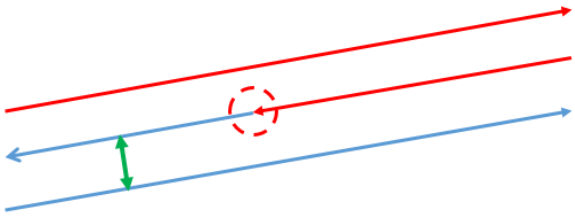

Figure 2.1: An example of the stepover distance for a toolpath. The red dashed ball represents the cutting tool. The green double headed arrow represents the stepover distance between successive passes.

Streamlines to Toolpaths - V0

This section describes the method of generating micrography based toolpaths first demonstrated by Pavanaskar et al. In order to go from streamlines to toolpaths, the first step is to offset the boundary. They first generate two boundary offsets: one contour at a distance of one tool radius (the center boundary offset) and another contour at a distance of two radii (the inner boundary offset). This serves to create the finishing passes for the pocket. The technique that is used to create the offsets is based on computing winding numbers (Chen and McMains, 2005). It works by constructing a raw offset curve of the region boundary and feeding that to the OpenGL Utility tesselator. They configure the tesselator such that it will remove areas with non-positive winding numbers. With the offset boundaries created, the next step is to trim the streamlines at the inner boundary offset. This is because the boundary offsets are the finishing passes of the toolpath and it is unnecessary to machine within the boundary offsets more than once. They trim the streamlines by first checking and keeping track of whether the first vertex of each streamline is inside or outside the boundary. Next, they loop through the vertices of each streamline to see if for a given vertex v_i, if the segment from $v_i \rightarrow v_{i+1}$ intersects the inner boundary. If it does, they flip the flag that keeps track of whether a vertex is inside or outside the boundary; otherwise, the value is maintained. After this is finished, they remove vertices that are outside of the inner boundary region. The nearest inner boundary vertex to the intersection point of a streamline and the inner boundary offset is added to the beginning or end of the trimmed streamline. The output of this method of trimming streamlines can be seen in Figures 2.2 (a) and (c). Once the streamlines are trimmed it is time to connect them into the final toolpath. This method of connecting them is a greedy approach that does not rely on the micrography line ordering. The code first starts at arbitrary trimmed streamline and searches from the end point for nearest the nearest untraversed streamline end point. If it can travel to nearest endpoint by traveling along the inner boundary, it does so and continues its search. Otherwise, it will air cut to that end point and continue its search. This repeats until all streamlines have been traversed. Figure 2.3 (a) shows the resulting toolpath.

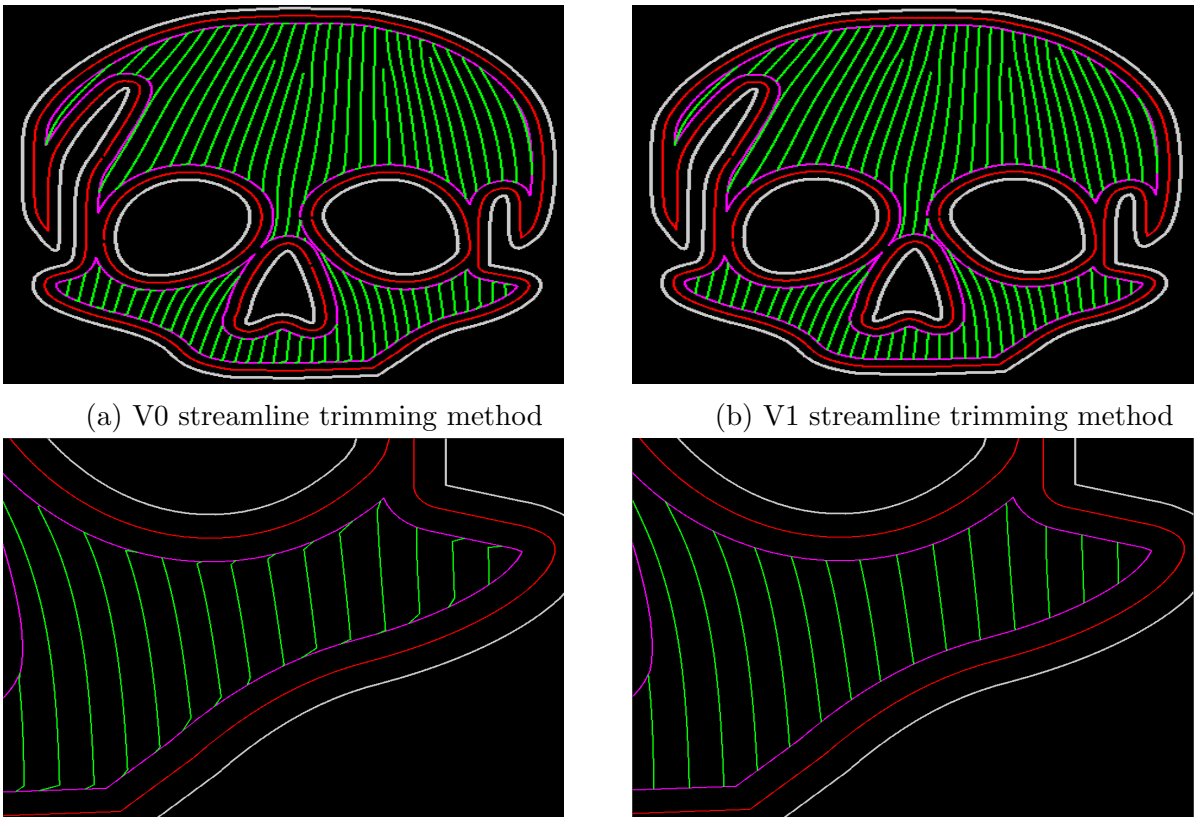

(a) V0 streamline trimming method

(b) V1 streamline trimming method

(c) Close-up: V0 streamline trimming method

(d) Close-up: V1 streamline trimming method

Figure 2.2: Comparison of streamline trimming methods

Streamlines to Toolpaths - V1

Here I present a new method of generating toolpaths from streamlines. It is very similar to the method previously described but makes some improvements that make it more energy efficient. The V0 approach travels along the boundary to go from streamline to streamline and this gives rise to scenarios where the tool will travel very far to the next streamline when it would be more energy efficient to air cut. It also adds the nearest inner boundary vertex to the streamline/inner boundary intersection point to the beginning and end of the trimmed streamlines. This can cause the streamlines to have a short and sharp corner at the end points. This effect can be seen in Figures 2.2 (a) and (c) in the bottom right region of the skull. A better approach to this is to add the actual intersection point between the pre-trimmed streamlines and the inner boundary offset so that the shape of the streamline is preserved (Figure 2.2 (d)). Finally, the V0 approach starts its search at an arbitrary streamline and traverses them solely based on distance from the current streamlines to the next one. Making use of the streamline ordering from micrography helps inform the search process.

Beginning with the boundary information, I generate the streamlines as described previ-

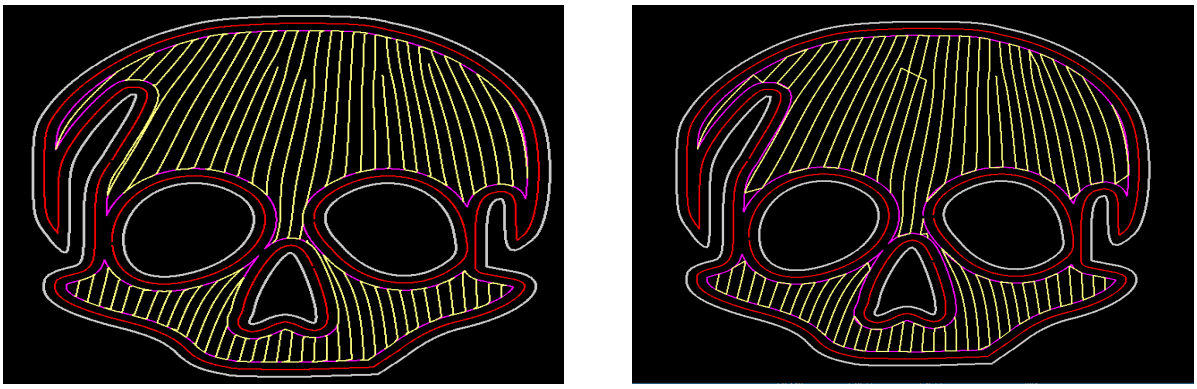

(a) V0 toolpath method (b) V1 toolpath method

Figure 2.3: Comparison of micrography toolpath methods

ously and save their ordering for later use. I then generate the boundary offsets. In order to trim the streamlines, I cast a horizontal ray to infinity from every vertex of every streamline. If the number of times a ray intersects the inner boundary offset is odd, a vertex is said to be within the boundary region and is not trimmed. I store a Boolean for whether a vertex is inside or outside the boundary for each vertex. I loop though the vertices of each streamline s_i and check whether the Boolean for vertex v_i is different from vertex v_{i-1}. If so, the streamline has crossed a boundary and I insert the intersection point of the segment $v_{i-1} \rightarrow v_i$ and the inner boundary offset to the beginning or end of the streamline, depending on whether the streamline is entering or exiting the inner boundary offset at that point. Vertices whose Boolean is false are outside of the inner boundary and are removed from their streamlines. The end result of the V1 trimming process can be seen in Figure 2.2 (b) and (d). It can be seen that the streamlines now retain their shape and don't make sharp turns as in the V0 approach. Once the streamlines are trimmed, they need to be ordered. Using the ordering index from the micrography process, I sort the trimmed streamlines into a list. If two streamlines were trimmed from the same pre-trimmed streamline, they retain the same ordering index as the original streamline and will appear adjacent to each other in the list.

Once the streamlines are trimmed, the process of creating the toolpath can now begin. Starting with the end point of the first ordered streamline, I calculate the distance to the nearest end point of the next ordered streamline. If this distance is less than a cut-off distance, the paths will be connected and the search will continue. The cut-off distance should be the smaller of the following two distances:

1. The distance that ensures that traveling between points will not damage the exterior part boundary

2. The distance where it becomes more energy efficient to air cut instead of traveling along the part

The energy efficient air cut distance would depend on a lot of factors specific to the machine, tool, cutting direction, and material. The G0 rapid movements in air cuts take virtually no additional energy as they take almost no time to complete. The energy efficiency limiting factors are the distance the tool has to travel before it can retract rapidly from the part, which is the same distance at which it plunges back into the material, and the feed rate used for plunging into the part. I currently only use the first condition in this work. The cutoff distance I use is 3.95R, where R is the tool radius, as it is one that ensures that the part will not be damaged. This is illustrated in Figure 2.4 and is proved as follows: Each streamline end point is guaranteed to be a minimum distance of 2R away from the pocket boundary because streamlines are trimmed at the inner boundary offset. Two points on opposite sides of the external boundary will always be a distance of 2R + the distance across the boundary + 2R away from each other. If we assume an infinitely thin pocket wall such that the distance across the boundary is zero, the closest the two points can ever be, while still being on opposite sides of the boundary, is 4R. Any distance less than this will result in end points being on the same side of the external boundary. Thus we can conclude that using a cut-off distance of 3.95R will ensure that the tool does not damage the part by clipping the external pocket boundary.

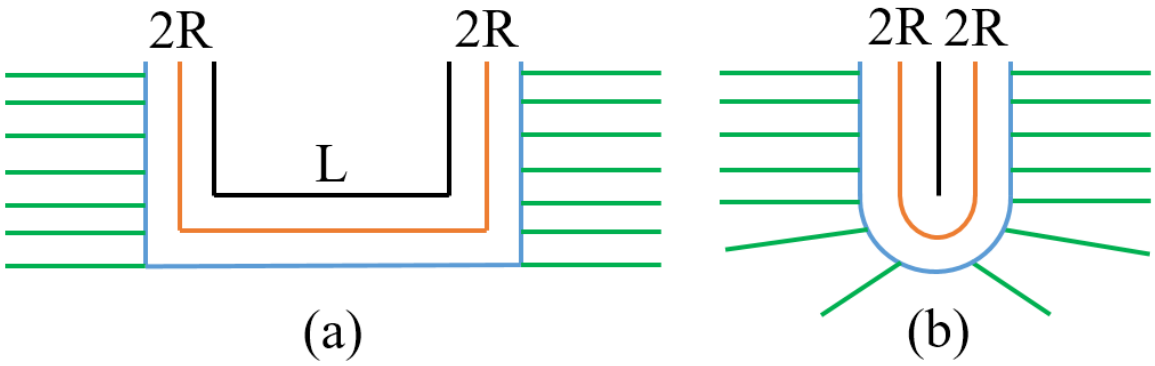

Figure 2.4: Diagram of streamlines and offset boundaries. (a) Streamlines (green) are trimmed at the inner boundary offset (blue). The inner boundary offset is a distance of 2R from the exterior part boundary (black). The distance across the part boundary is denoted as L. (b) Streamlines and boundary offsets drawn with an infinitely thin part boundary

If the distance between the current streamline end point and the nearest end point of the next ordered streamline is greater than the cutoff distance, I loop through the remaining non-traversed streamlines in order and check the end points of those streamlines until an end point within this cut-off distance is found. If no such end point is found, the toolpath will air cut to the first end point that was checked and the search will continue until all streamlines have been traversed. Because trimming can split a streamline into multiple streamlines, and those streamlines are given the same order, if when generating the toolpath the current streamline and the next streamline share the same order ID, I push the next streamline to the back of the list. The resulting toolpath can be seen in Figure 2.3 (b) above.

2.2 Machining and Recording Energy

Generating Commercial Toolpaths for Fair Comparison

Testing whether micrography based toolpaths are more energy efficient than commercial toolpath approaches requires a method of generating commercial toolpaths that allow for a fair comparison. One such method is by attempting to keep the typical instantaneous material removal rate the same between all toolpaths that are to be tested. This can be done by keeping the feed rates as well as the spindle speed the same, and by using the same stepover distance. Using a smaller stepover will result in the tool making more back-and-forth passes and thus the toolpath will consume more energy. I generate micrography based toolpaths and calculate their stepover. I give the calculated stepover distance and other parameters as input to the commercial CAM software MasterCAM X9 to generate toolpaths for the machining comparison experiments. The stepover distance for micrography based toolpaths can be calculated by sampling the distance between streamlines all over the part. Very simply, it can be accomplished by repeating the following for n samples and averaging the result (pseudocode provided in Algorithm 1):

1. Choose a random vertex v_i from a random ordered streamline s_i
2. Create a segment p perpendicular to segment $v_i \rightarrow v_{i+1}$ centered at the midpoint of segment $v_i \rightarrow v_{i+1}$
3. Loop through the line segments of s_{i+1} and look for an intersection with p
4. If an intersection exists, the distance from the midpoint of segment $v_i \rightarrow v_{i+1}$ to the intersection point is the stepover distance

In order to determine the appropriate sample size such that the stepover distance calculation reaches an asymptote, I ran the algorithm on the ordered streamlines for the skull shape generated for a tool of radius 2.3813 mm (3/32 in) with varying sample sizes. For each sample size I performed five trials and plotted the averages against the sample size in Figure 2.5 below. It can be seen that the stepover distance begins to have little variation at about 2,500 samples and approaches a value of 2.62 mm (0.103 in). For the bear shape with a tool radius of 1.1902 mm (3/64 in), the stepover is approximately 1.27 mm (0.50 in).

Milling Experiments

I repeated a set of cutting experiments performed by Pavanaskar et al. 2015 on a different CNC machine to see if the energy savings they found for micrography based toolpaths could also be had on a different configuration. They compared various commercial toolpaths to a micrography based toolpath generated for a bear shape on a Haas VF-0 CNC machine. I converted the toolpaths that they used to metric units and translated the origin such that the toolpaths could be cut on the Mori. I changed the feeds and speeds to values

Algorithm 1: Sampling the stepover distance between ordered streamlines

Input : Set of ordered streamlines $S = \{s_0, s_1, s_2, ..., s_n\}$
Output: Stepover distance sample

```
finished ← False ;
R ← Tool radius ;
while not finished do
    s_i ← random ordered streamline from S ;
    v_i ← random vertex from s_i ;
    p_i ← segment with length 6R perpendicular to v_i → v_{i+1} and centered at
     the midpoint of segment v_i → v_{i+1} ;
    for v_j ∈ s_{i+1} do
        p_j ← segment from v_j → v_{j+1} ;
        if intersect(p_i, p_j) then
            return distance from midpoint of p_i → intersection
        end
    end
end
```

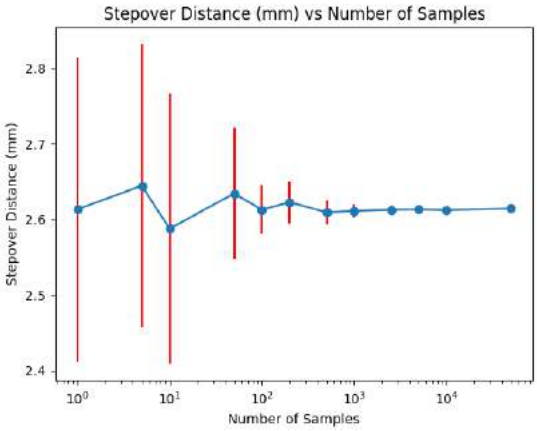

Figure 2.5: Calculated stepover distance plotted against the number of samples

more appropriate for the Mori; they can be found listed in Table 2.1 below. I machined the adjusted toolpaths on the Mori and all toolpaths were cut on the same block of 6061 aluminum. After a toolpath experiment was run, I faced the stock material to provide a fresh surface for another experiment. I recorded the power consumption of all cutting experiments using a Yokogawa CW240 power meter connected directly to the Mori. The Yokogawa CW240 can record three phase voltage, current, and instantaneous power and was set to sample every 100 ms.

In addition to repeating experiments performed by Pavanaskar et al., I also generated

toolpaths for the bear and skull shapes. For each geometry, I generated two toolpaths using the V0 and V1 micrography approaches, as well as commercial toolpaths in MasterCAM X9 and kept the stepover distances (calculated previously) and parameters (Table 2.2 for the skull and Table 2.1 for the bear) the same. As before, I machined the toolpaths for each geometry out of the same piece of stock material and faced it after each experiment. I recorded the power consumption of these experiments using the Yokogawa CW240.

Power Data Processing and Integration

Tonissen reported that the power consumption of the Mori CNC is dependent on the previous state of the machine (2009). When the machine is hot, the cooling systems work hard to maintain a suitable temperature and the overall power consumption is greater. In order to try and eliminate this system level fluctuation, I offset the power data of each experiment by subtracting the average power consumption of the machine when idle just prior to that specific experiment. An example of a time-power curve and the value used as an offset is provided in Figure 2.6 below. Pavanaskar et al. computed the energy consumption by first smoothing the time-power curve as recorded by the Yokogawa CW240 using a moving average, and then integrating. Smoothing the curve has a tendency to remove energy spikes due to air cuts and other machine level power demands. I integrate the time-power curve after offsetting using the trapezoidal rule with strip width of 100 ms (integrate between all samples) without smoothing. Energy values when integrating with and without smoothing differ by less than a quarter of a percent (for a full comparison see Table 5.1 in the appendix).

Table 2.1: Bear experiment parameters

Parameters	Haas VF-0	Mori NVD 1500 DCG
Tool diameter (in)	3/32	3/32
Depth of cut (mm)	-1.778	-1.778
Height of air cut (mm)	2.54	2.54
Spindle speed (rev/min)	5,000	35,000
Feed rate (mm/min)	381	890
Down feed rate (mm/min)	101.6	300

Table 2.2: Skull experiment parameters

Parameters	Mori NVD 1500 DCG
Tool diameter (in)	3/16
Depth of cut (mm)	-1.778
Height of air cut (mm)	2.54
Spindle speed (rev/min)	17,300
Feed rate (mm/min)	900
Down feed rate (mm/min)	450

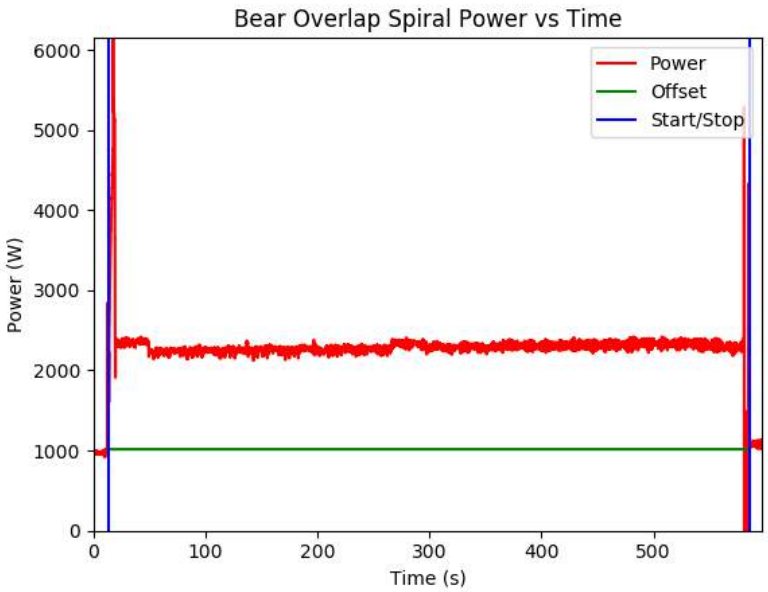

Figure 2.6: Plot of power vs. time with average idle power offset

Chapter 3

Results and Discussion

3.1 Repeating Bear Experiments

The results of the bear cutting experiment repetitions are provided in Table 3.1. The energy values for the experiments performed on the Haas are as reported by Pavanaskar et al. (2014). The energy values for the experiments performed on the Mori are lower, but this is explained by lower cycle times on the Mori due to the higher feedrates used in the experiments. The idle power consumption of the Haas is around 300W and 1000W for the Mori, so this would not account for the lower energy consumption on the Mori. To allow the relative energy consumption to be seen, I normalize the energy values for each machine by the energy consumed by the V0 micrography toolpath (Table 3.2). The V0 micrography toolpath still outperformed the constant overlap spiral and the zigzag toolpaths on the Mori. It is possible that the difference in relative performance between toolpaths is due to differences in energy consumption and configuration between machines, as well as the variability of the machine state itself.

Table 3.1: Machine Comparison

Toolpath	Haas VF-0 Energy (J)	Mori NVD 1500 DCG (J)
Const. Overlap Spiral	2,548,804	725,484.9
Zigzag	2,487,383	708,704.0
V0 Micrography	1,975,765	523,413.8

Table 3.2: Normalized Energy Machine Comparison

Toolpath	Haas VF-0	Mori NVD 1500 DCG
Const. Overlap Spiral	1.29	1.38
Zigzag	1.26	1.35
V0 Micrography	1	1

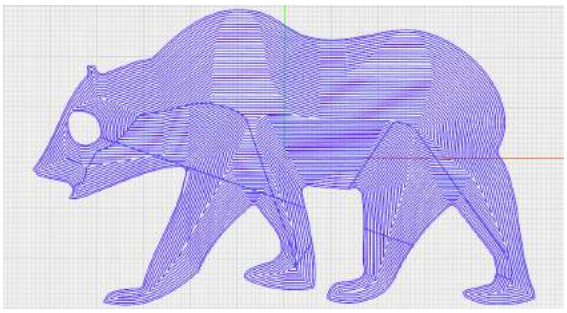

(a) Bear Overlap Spiral Toolpath

(b) Bear Overlap Spiral Result

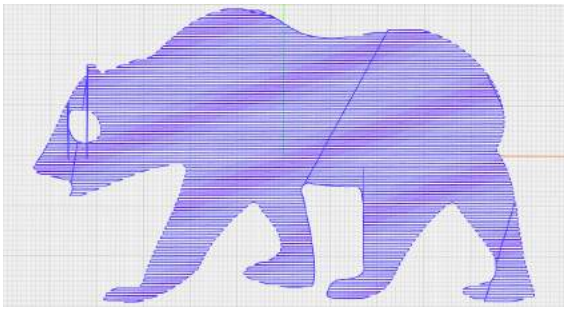

(c) Bear Zigzag Toolpath

(d) Bear Zigzag Result

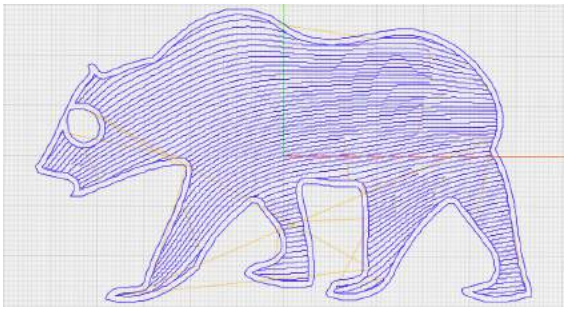

(e) Bear V0 Micrography Toolpath

(f) Bear V0 Micrography Result

Figure 3.1: Bear toolpaths and machined results

A visualization of the toolpaths machined on the Mori (visualized using the online tool NC Viewer (Luciano, 2018)) and the machined results can be seen in Figure 3.1. Although the surface roughness of the toolpaths do not seem to vary greatly, the surface finish of the micrography toolpath is less visually appealing than the others. This is because the micrography toolpath generated by Pavanaskar et al. was based on boundary information and streamlines provided by the authors of the Digital Micrography work. In order to turn them into a machinable toolpath, they needed to be scaled down significantly, and in the process of doing so, significant figures were lost. The loss of accuracy led to severe aliasing that can be seen in Figure 3.2. This aliasing is likely what is responsible for the poor surface finish. Plots of the time-power curve for each of the machined toolpaths are provided in appendix Figure 5.3. All three toolpaths can be seen to have a very similar mean power

consumption. The micrography toolpath saves more energy because it is able to finish more rapidly than the others.

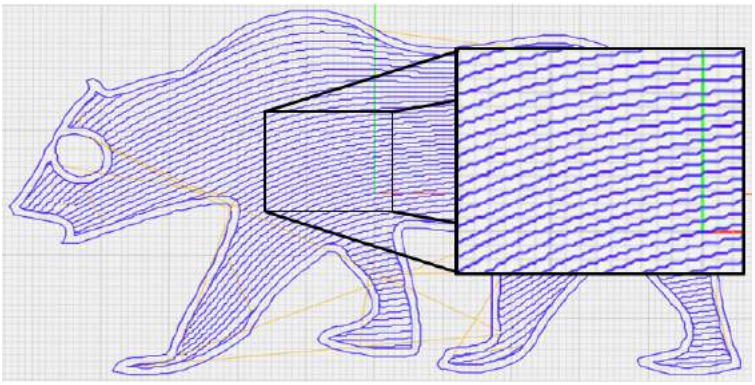

Figure 3.2: Micrography toolpath generated by Pavanaskar et al. with close-up of streamline aliasing

3.2 Comparison

In the previous section it was shown that the V0 micrography toolpath outperforms the commercial toolpaths by approximately 30 to 40 % when the experiments performed by Pavanaskar et al. are repeated. The toolpaths that Pavanaskar et al. generated used the same parameters and stepover distance in order to ensure a fair comparison by keeping the instantaneous material removal rate as similar as possible. Pavanaskar et al. report calculating the stepover distance for the V0 micrography toolpath for the bear shape as 0.023 in. This was done in a similar fashion to the method for calculating streamline stepovers described previously. They then report using this stepover distance to generate toolpaths in MasterCAM. A side-by-side comparison of the toolpaths that were machined, however, shows that the stepover distances are not as similar as reported. It can be seen in Figure 3.3 (a) that the toolpaths generated by Pavanaskar et al. appear to have dissimilar stepover distances. The zigzag and overlap spiral toolpaths appear to have stepovers that are much smaller than the V0 micrography toolpath. I took 6 samples from various locations of the bear zigzag toolpath and averaged the distances resulting in a stepover distance of 0.0186 in. Five of the six samples were identical, and the different passes of the toolpath had high uniformity leading to a high degree of confidence in the result. I then took and averaged 7 samples from all over the original micrography bear toolpath resulting in a stepover of 0.033 in, which is approximately 43 % higher than initially reported by Pavanaskar et al. This toolpath is more irregular than the zigzag toolpath and as such, it cannot be said with certainty that this stepover distance is accurate. This however illustrates that without an adequate number of samples, confidence cannot be had in the stepover distance. The

smaller stepovers of the commercial toolpaths resulted in more back-and-forth passes than the micrography toolpath, and therefore, resulted in more energy being consumed during the machining process.

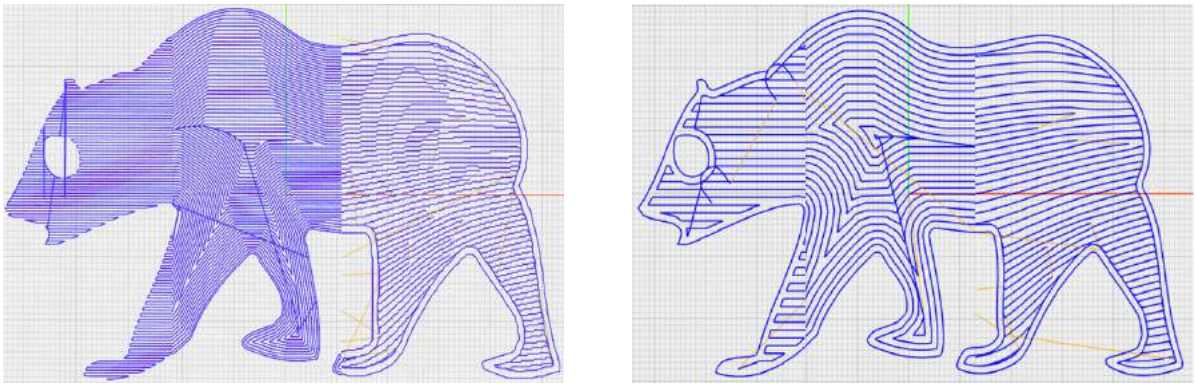

(a) Composite image of bear toolpaths as generated by Pavanaskar et al.

(b) Composite image of bear toolpaths with improved stepovers that I generated

Figure 3.3: Comparison of toolpath stepovers for the bear geometry

For the same geometry, I regenerated micrography toolpaths (both V0 and V1) for a 3/64 in. tool and calculate a stepover of 0.050 in. This stepover distance is then used to generate zigzag and overlap spiral toolpaths in MasterCAM X9. A composite image of the toolpaths is provided in Figure 3.3 (b). It can be seen that the stepovers for these toolpaths are far more similar than those previously generated. I machined these new toolpaths and recorded the energy consumption of the experiments. The toolpaths and pictures of the machined pockets are provided in appendix Figure 5.5 and the time-power plots are provided in appendix Figure 5.4. The surface finish for all pockets in this set are more similar than that of the first set of bear cutting experiments. Streamline aliasing was avoided because I generated the micrography toolpaths for the pocket such that scaling was unnecessary. The results of the experiments are provided in Table 3.3. It can be seen that the V1 micrography approach is about 4 % more energy efficient than the V0 approach. This improvement is enabled by the fact that the V1 approach avoids many long segments where the tool traverses the boundary to reach the next streamline as in the V0 approach. The V0 and V1 micrography approach were both less energy efficient than the zigzag and overlap spiral toolpaths, however, the discrepancy between the results of this set of toolpath comparisons and the previous can be explained by the differences in stepover and the fact that the zigzag toolpath does not rely on an additional contour pass to cut all the material in the pocket like the V0 and V1 micrography toolpaths do. This additional contour pass (the inner boundary offset) is an artifact of the streamline generation and processing step and is currently necessary to ensure 100 % of the material is removed during machining. This is due in part to another shortcoming of the micrography streamlines, which is that they do not extend all the way to the boundary. The shortcoming becomes problematic when attempting to create a toolpath

without including the inner boundary offset as a contour finish pass because material is left uncut. We cannot currently offset the boundary before generating the streamlines because the processes of generating boundary offsets and streamline generation are not commutative, so generating streamlines for the entire boundary and then trimming at the inner boundary offset gives a different result than generating the streamlines for the offset region. Neither result is successful at removing 100 % of the pocket material without the extra contour pass. I propose several improvements to the micrography toolpath approaches. The first is to generate the streamlines for the inner boundary offset instead of for the entire region. This will eliminate the need to trim the streamlines at the inner boundary and will increase the uniformity of the streamlines in the area of interest. The second is to improve the streamlines such that including the inner boundary offset as a part of the toolpath becomes unnecessary. Improvements will include ensuring that the streamlines extend all the way to the whichever boundary they are being generated for, and increasing the uniformity of the spacing. This will save time and in turn make the microraphy based toolpath more energy efficient.

Table 3.3: Fair Energy Comparison on Mori NVD 1500 DCG

Toolpath	Energy (J)	Normalized Energy
Const. Overlap Spiral	578,167.0	1.03
Zigzag	559,118.5	1
V1 Micrography	652,962.5	1.12
V0 Micrography	626,814.5	1.16

3.3 Influence of Geometry and Machining Axis

In order to test whether the performance of the micrography toolpaths is consistent between geometries and primary machining directions, I generated toolpaths based on both micrography approaches and a constant overlap spiral in MasterCAM for a pocket in the shape of a skull. These toolpaths were loaded onto the CNC machine. I performed two sets of cutting experiments. One set had the pocket oriented such that the primary machining direction was aligned with the Y-axis, and the other set had the pocket rotated 90 degrees using a G68/G69 (rotation) command embedded in the toolpaths such that the primary machining direction was aligned with the X-axis. The toolpaths used and the machined results for the Y-aligned experiments can be seen in Figure 3.5. The Y-aligned pocket cut using the V1 micrography toolpath had slightly noticeable ridges across the pocket, but this is likely due to the stock flexing during machining since it was quite thin (around 1/8 in). One of the parallels came loose during machining and likely contributed to the increased surface roughness. The time-power curve for each toolpath can be seen in appendix Figures 5.6. As in the previous case, each toolpath has a similar mean power consumption and as such, the energy consumed is determined by the machining time. Bar charts comparing the machining time and energy consumption for each primary axis are provided in Figure 3.4. The values

used to generate these plots are provided in appendix Table 5.2. There do not appear to be significant energy consumption differences when machining aligned primarily in the X or Y direction. This is consistent with previous work performed on the Mori that showed that the difference in energy consumed while cutting in the X and Y direction is not large (Budinoff, 2015). Tonissen performed experiments on the Mori and found that cuts aligned with the Y axis were more energy efficient than cuts in the X axis. He also reported that cutting with both axes simultaneously consumed more energy than cutting with just one (2009). The toolpaths I generated all feature movements that require the motion of both X and Y axes simultaneously, which may contribute to the lack of major differences in energy consumption. Tonissen did not report the sample size for his experiments and mentioned that there is a great degree of variability when performing cutting experiments on the machine. It is likely that the offsetting of the power-data by the mean idle power consumption prior to the experiment is not sufficient to remove machine variability effects and this has likely manifested itself in the data. Figure 3.4 (a) appears to show that machining aligned with the X axis is marginally more energy efficient than when aligned with the Y axis, however the trend shifts for the V0 micrography toolpath. I only performed six experiments, resulting in a samplie size of one for each toolpath, per axis, and therefore I cannot conclude reliably whether axis mounting really is a significant consideration when seeking to machine in an energy efficient manner. The constant overlap spiral outperformed both of the micrography based toolpaths. Despite having the same stepover distance and using the same parameters as the micrography based toolpaths, it was still faster and more energy efficient. This is consistent with the findings in the previous section.

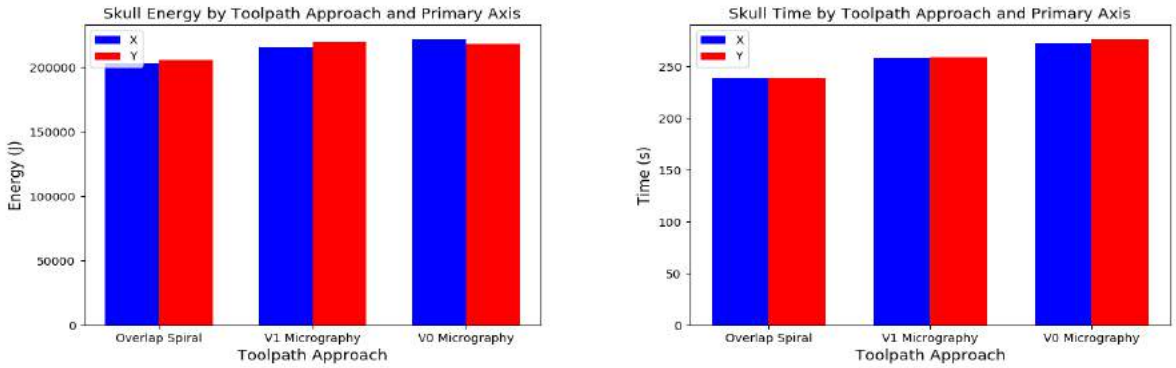

(a) Toolpath primary axis energy comparison. Bar colors: [Blue: X, Red: Y]

(b) Toolpath primary axis time comparison. Bar colors: [Blue: X, Red: Y]

Figure 3.4: Bar charts comparing energy and time usage by toolpath approach and primary axis

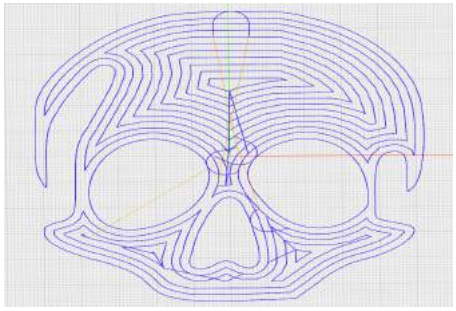

(a) Skull Spiral Toolpath

(b) Skull Overlap Spiral Result

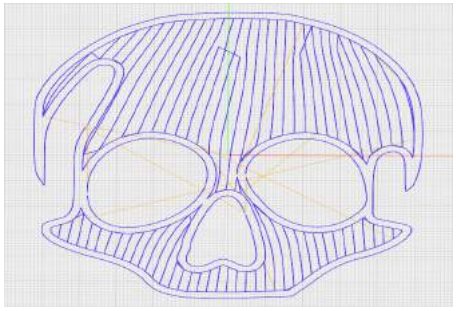

(c) Skull New Micrography Toolpath

(d) Skull New Micrography Result

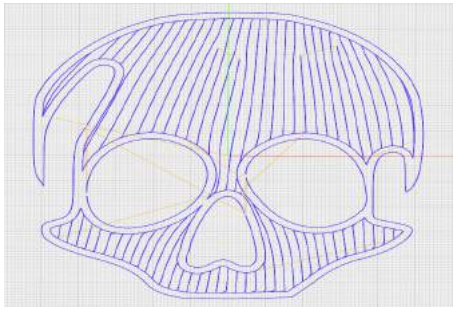

(e) Skull Old Micrography Toolpath

(f) Skull Old Micrography Result

Figure 3.5: Skull toolpath and machined results

Chapter 4

Conclusions

This report described an improved method of using streamlines based on digital micrography to generate toolpaths. This work investigated previously reported energy savings when using micrography based toolpaths and demonstrated that although vector field based toolpaths have potential for energy efficiency, it cannot said for certain that these micrography based toolpaths are inherently more energy efficient. Streamline generation and boundary processing is not commutative, and this results in the quality of the micrography based toolpaths being dependent on the order that toolpath generation operations are performed. Work needs to be done to improve the uniformity of the streamlines so the inner boundary offset does not need to be added as a contour finish pass. This extra contour pass results in higher process time and less energy efficiency. Furthermore, the restrictions placed on the alignment of the streamlines to the boundary, while necessary for the layout of legible text on an image, can actually hinder energy performance. In micrography's current form, streamlines will not align with the boundary of pocket geometries with high amounts of curvature. This results in streamlines that when connected begin to resemble zigzag toolpaths. It is possible that using the medial axis of a pocket to inform the creation of a vector field can lead to streamlines that are more energy efficient. It is important for designers and engineers who are concerned about energy efficiency to consider the geometry of the pocket when choosing an appropriate toolpath. Toolpath approaches are not "one size fits all."

Chapter 5

Appendix

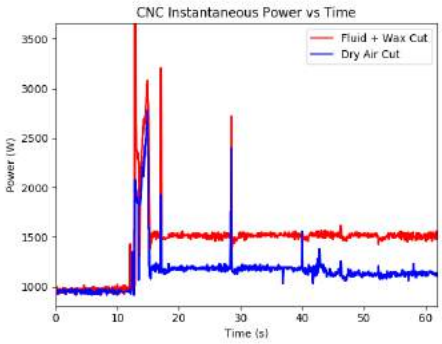

Figure 5.1: Power consumption for milling operations on a Mori Seiki NVD 1500: (a) dry air cut [blue] (b) lubricated wax cut [red]

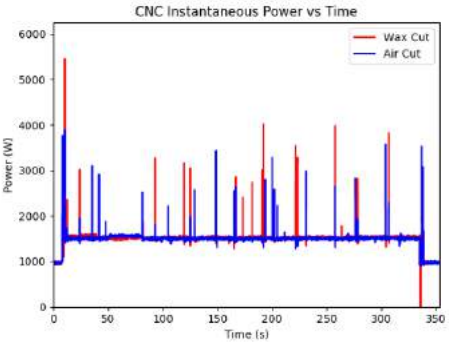

Figure 5.2: Power consumption for milling operations on a Mori Seiki NVD 1500: (a) air cut [blue] (b) wax cut [red]

Using the data recorded in the experiments performed by Pavanaskar et al., I integrated the time-power curve using the trapezoidal rule without smoothing. My calculations varied very little except for the energy of the micrography based toolpath. This discrepancy is likely due to mislabeled data. The paper reports that this toolpath took 1013 seconds to machine, however the power data provided only has about 850 seconds of data.

Table 5.1: Power Curve Integration Comparison

Toolpath	Given Energy (J)	Calc. Energy (J)	% Difference
Const. Overlap Spiral	2,548,804	2,544,470	0.17
X-Parallel	2,576,525	2,572,718	0.15
Parallel Spiral	2,545,579	2,544,472	0.04
Y-One Way	3,054,194	3,052,979	0.04
Zigzag	2,487,383	2,484,128	0.13
Micrography	1,975,765	1,672,624	16.62

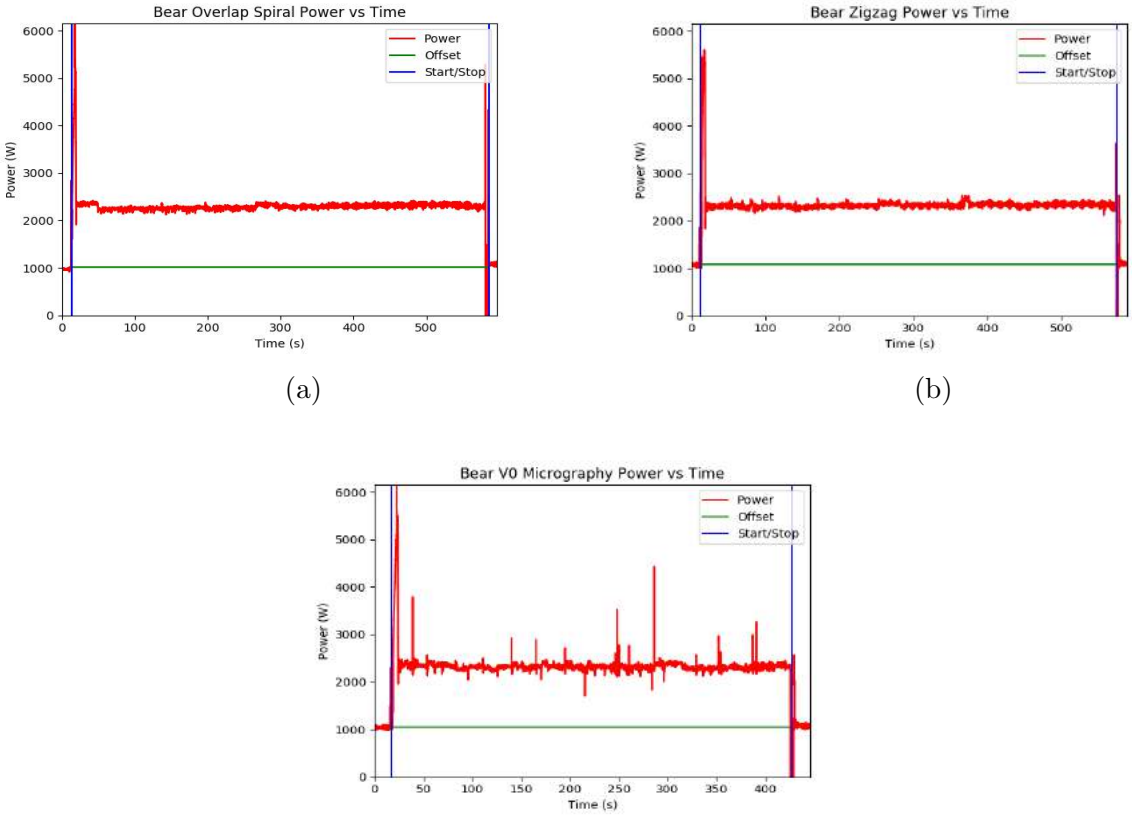

Figure 5.3: Power and time plotted for the bear shape given the following toolpaths: (a) overlap spiral; (b) zigzag; and (c) V0 micrography.

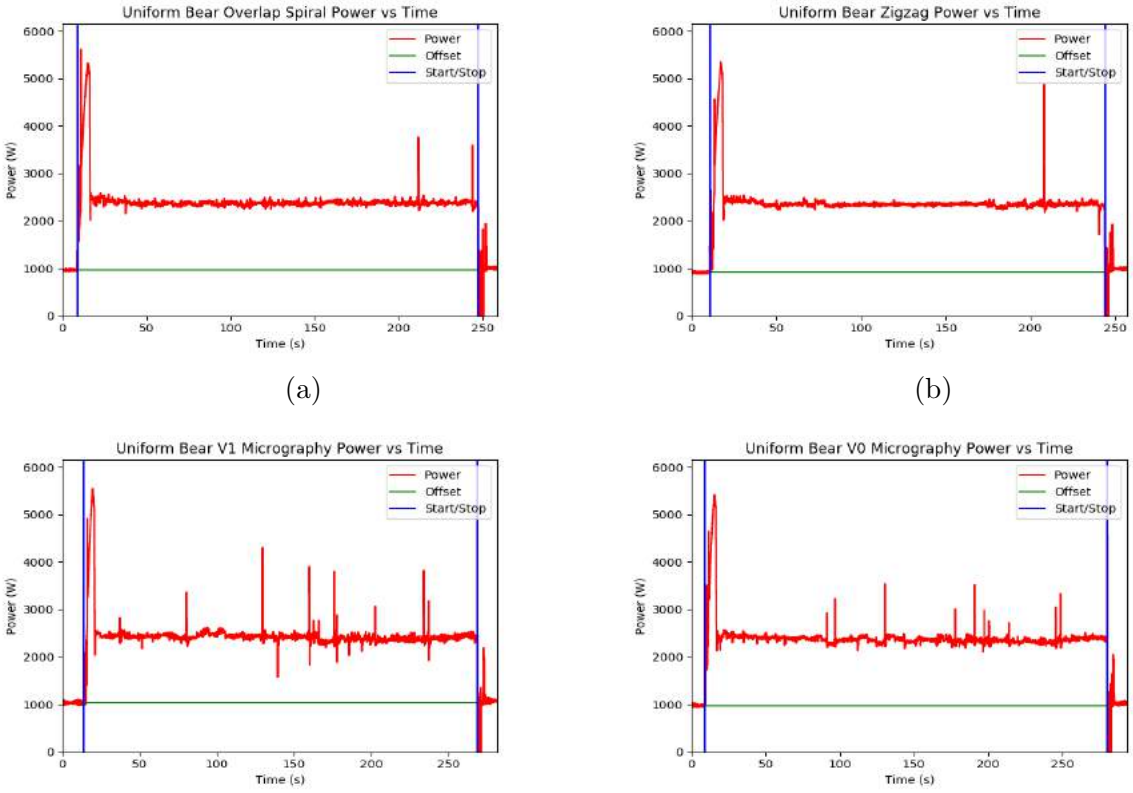

Figure 5.4: Power and time plotted for the bear shape given the following toolpaths: (a) overlap spiral; (b) zigzag; (c) V1 micrography; and (d) V0 micrography.

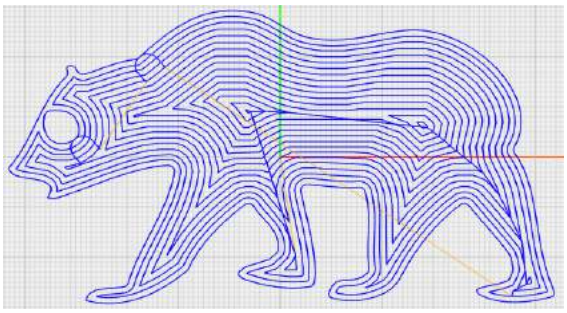

(a) Uniform Bear Overlap Spiral Toolpath

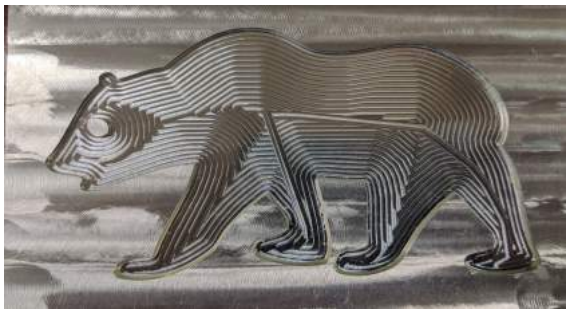

(b) Uniform Bear Overlap Spiral Result

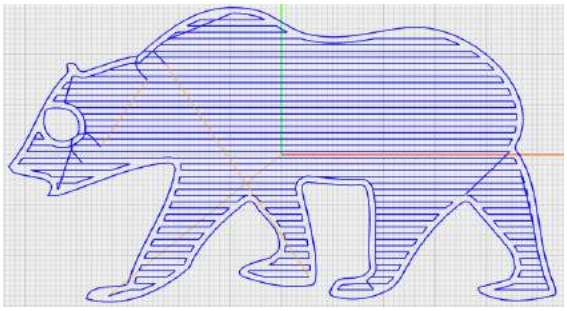

(c) Uniform Bear Zigzag Toolpath

(d) Uniform Bear Zigzag Result

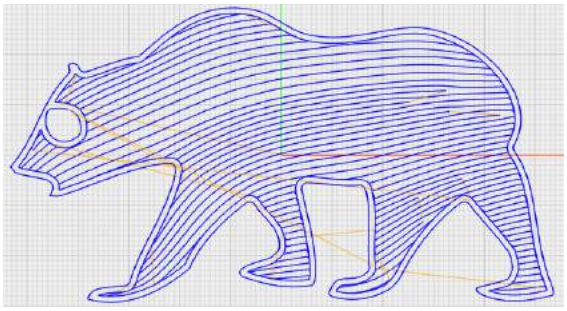

(e) Uniform Bear V0 Micrography Toolpath

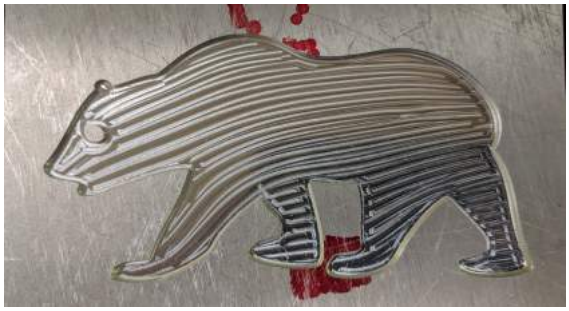

(f) Uniform Bear V0 Micrography Result

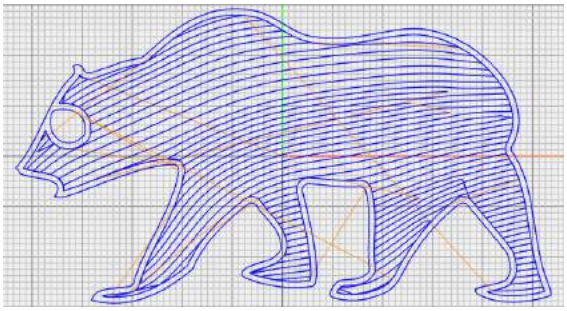

(g) Uniform Bear V1 Micrography Toolpath

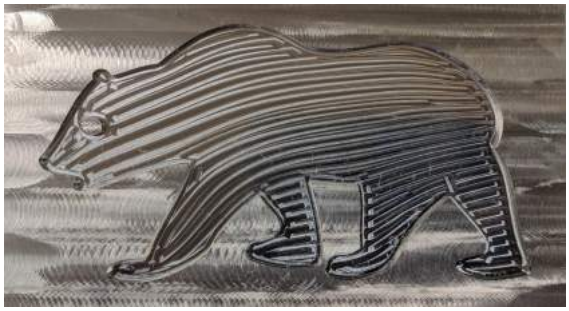

(h) Uniform Bear V1 Micrography Result

Figure 5.5: Uniform bear toolpaths and machined results

Table 5.2: Skull Toolpath Comparison: X and Y Primary Axes

Toolpath	Energy Y (J)	Energy X (J)	Time Y (s)	Time X (s)
Const. Overlap Spiral	436,289.5	430,857.5	238.6	238.6
V1 Micrography	472,152.5	465,997.5	258.3	258.0
V0 Micrography	482,382.0	488,061.0	276.3	272.7

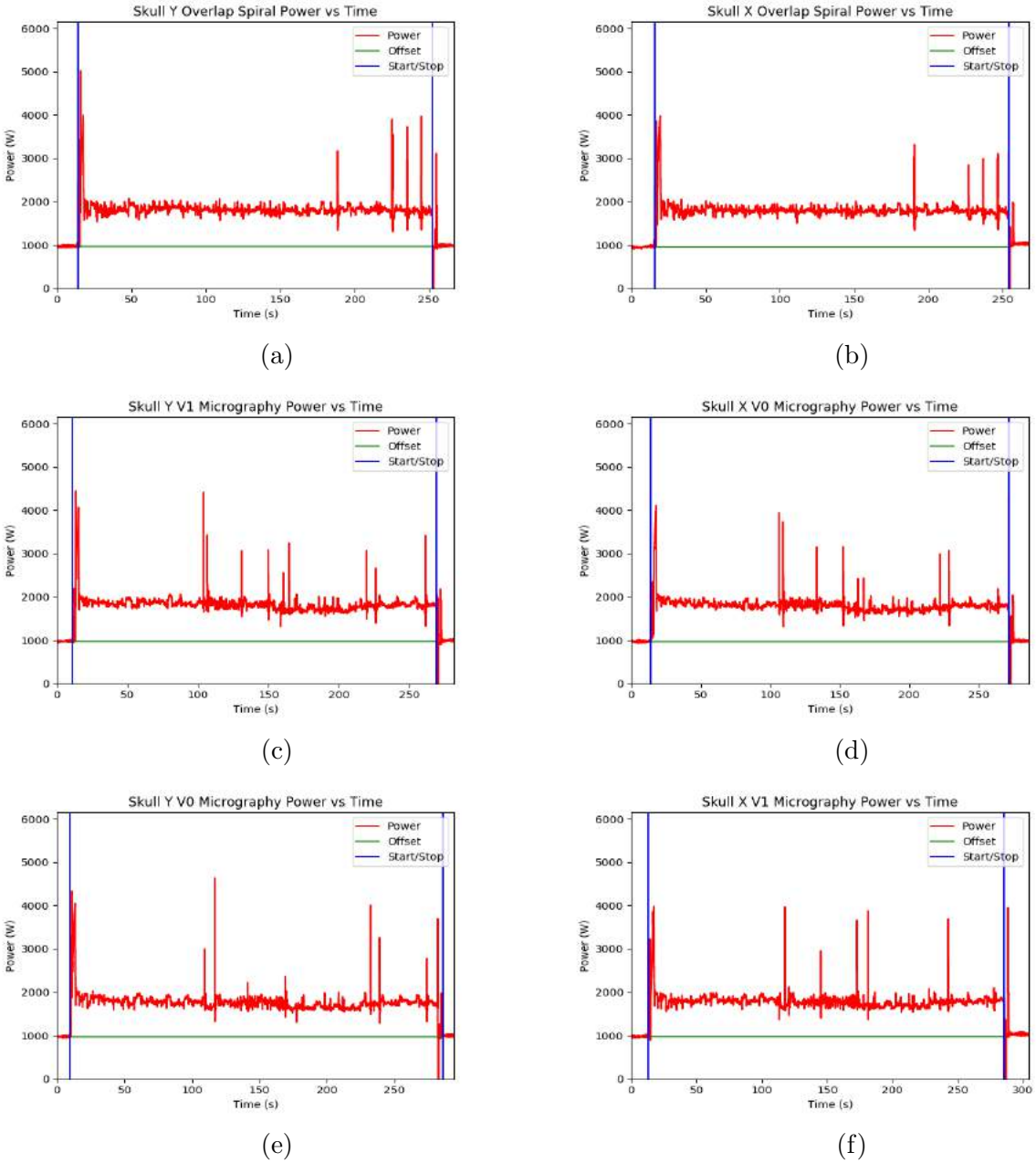

Figure 5.6: Power and time plotted for the skull shape machined given the following toolpaths: (a) overlap spiral aligned with Y; (b) overlap spiral aligned with X; (c) V1 micrography algined with Y; (d) V1 micrography algined with X; (e) V0 micrography algined with Y; and (f) V0 micrography aligned with X.

Bibliography

U.S. Energy Facts - Energy Explained (2017). URL: https://www.eia.gov/energyexplained/index.php?page=us_energy_use (visited on 06/21/2018).

U.S. Energy Facts - Energy Explained (2018). URL: https://www.eia.gov/energyexplained/index.php?page=us_energy_industry (visited on 07/25/2018).

Kordonowy, David N. (2002). "A Power Assessment of Machining Tools". Bachelor's Thesis. Massachusetts Institute of Technology.

Pavanaskar, Sushrut (2014). "Improving Energy Efficiency in CNC Machining". PhD thesis. URL: https://escholarship.org/uc/item/80t8k1qj (visited on 06/21/2018).

Pavanaskar, Sushrut et al. (2015). "Energy-efficient vector field based toolpaths for CNC pocketmachining". In: *Journal of Manufacturing Processes* 20.Part 1, pp. 314–320. ISSN: 1526-6125. DOI: 10.1016/j.jmapro.2015.06.009.

He, Y et al. (2012). "Analysis and estimation of energy consumption for numerical control machining". In: *Proceedings of the Institution of Mechanical Engineers, Part B: Journal of Engineering Manufacture* 226.2, pp. 255–266. DOI: 10.1177/0954405411417673.

Gutowski, Timothy et al. (2005). "Environmentally benign manufacturing: Observations from Japan, Europe and the United States". In: *Journal of Cleaner Production* 13.1, pp. 1–17. ISSN: 0959-6526. DOI: 10.1016/j.jclepro.2003.10.004.

Diaz, Nancy, Elena Redelsheimer, and David Dornfeld (2011). "Energy Consumption Characterization and Reduction Strategies for Milling Machine Tool Use". In: *Glocalized Solutions for Sustainability in Manufacturing*. Berlin, Heidelberg: Springer Berlin Heidelberg, pp. 263–267. ISBN: 978-3-642-19692-8.

Tonissen, Stefan (2009). "Power Consumption of precision machine tools under varied cutting conditions". Master's Thesis. RWTH Aachen University, Berkeley.

Minquiz, G.M. et al. (2016). "A Comparative Analysis Between High Speed Dynamic and Traditional Pocketing Toolpaths in Precision Milling Machines". In: *International Manufacturing Science and Engineering Conference* 3. DOI: 10.1115/MSEC2016-8746.

Huang, Nuodi, Roby Lynn, and Thomas Kurfess (2017). "Aggressive Spiral Toolpaths for Pocket Machining Based on Medial Axis Transformation". In: *Journal of Manufacturing Science and Engineering* 139.5, pp. 051011-0-51011-8. ISSN: 1087-1357. DOI: 10.1115/1.4035720.

Maharik, Ron et al. (2011). "Digital Micrography". In: *ACM SIGGRAPH 2011 Papers*. SIGGRAPH '11. Vancouver, British Columbia, Canada: ACM, 100:1–100:12. ISBN: 978-1-4503-0943-1. DOI: 10.1145/1964921.1964995.

Palacios, Jonathan and Eugene Zhang (2007). "Rotational Symmetry Field Design on Surfaces". In: *ACM SIGGRAPH 2007 Papers*. SIGGRAPH '07. San Diego, California: ACM. DOI: 10.1145/1275808.1276446.

Chen, Xiaorui and Sara McMains (2005). "Polygon Offsetting by Computing Winding Numbers". In: *ASME 2005 International Design Engineering Technical Conferences and Computers and Information in Engineering Conference*. Vol. 2: 31st Design Automation Conference, Parts A and B. ASME, pp. 565–575.

Luciano, Xander (2018). *NC Viewer - Online Gcode Viewer*. URL: https://ncviewer.com/ (visited on 06/21/2018).

Budinoff, Hannah (2015). "Predicting Energy Usage During Milling Milling Based on Workpiece Orientation". Master's Report. University of California, Berkeley.